

**OPEN ACCESS**

## Gain dynamics and saturation in semiconductor quantum dot amplifiers

To cite this article: T W Berg *et al* 2004 *New J. Phys.* **6** 178

View the [article online](#) for updates and enhancements.

### You may also like

- [TE-mode nonreciprocal propagation in passive Fe<sub>0.6</sub>Co<sub>0.4</sub>-InGaAsP/InP semiconductor optical isolators](#)  
Hiromasa Shimizu, Shohei Sakanishi, Takahiro Bando et al.
- [Theory of four-wave mixing in quantum dot semiconductor optical amplifiers](#)  
Ahmed H Flayyih and Amin H Al-Khursan
- [Roadmap on all-optical processing](#)  
Paolo Minzioni, Cosimo Lacava, Takasumi Tanabe et al.

## Gain dynamics and saturation in semiconductor quantum dot amplifiers

**T W Berg, J Mørk and J M Hvam**

Research Center COM, Technical University of Denmark, Build. 345V,  
2800 Lyngby, Denmark  
E-mail: [twb@com.dtu.dk](mailto:twb@com.dtu.dk)

*New Journal of Physics* **6** (2004) 178

Received 3 June 2004

Published 26 November 2004

Online at <http://www.njp.org/>

doi:10.1088/1367-2630/6/1/178

**Abstract.** Quantum dot (QD)-based semiconductor optical amplifiers offer unique properties compared with conventional devices based on bulk or quantum well material. Due to the bandfilling properties of QDs and the existence of a nearby reservoir of carriers in the form of a wetting layer, QD semiconductor optical amplifiers may be operated in regimes of high linearity, i.e. with a high saturation power, but can also show strong and fast nonlinearities by breaking the equilibrium between discrete dot states and the continuum of wetting layer states. In this paper, we analyse the interplay of these two carrier populations in terms of a simple rate equation model. Based on the steady-state and small-signal properties of the model, we analyse and discuss the optical modulation response and the four-wave mixing properties of QD semiconductor optical amplifiers, in particular emphasizing the role of ultrafast gain dynamics.

**Contents**

<b>1. Introduction</b>	<b>2</b>
<b>2. The model</b>	<b>3</b>
<b>3. Continuous wave (CW) properties of QD amplifiers</b>	<b>5</b>
3.1. Filling of the active states . . . . .	6
3.2. Saturation power . . . . .	7
<b>4. Small signal analysis</b>	<b>10</b>
<b>5. Optical modulation response</b>	<b>12</b>
5.1. Size of the modulation response . . . . .	12
5.2. Phase of the modulation response . . . . .	15
<b>6. Four-wave mixing</b>	<b>16</b>
6.1. A simple model . . . . .	16
6.2. FWM results . . . . .	18
<b>7. Conclusion</b>	<b>21</b>
<b>Acknowledgments</b>	<b>22</b>
<b>Appendix. Parameter values</b>	<b>22</b>
<b>References</b>	<b>22</b>

**1. Introduction**

It has been demonstrated over the past few years that the use of quantum dot (QD) active material may improve the properties of semiconductor lasers [1, 2] as well as semiconductor optical amplifiers (SOAs) [3]. Early predictions on the performance of QD based opto-electronic devices [4] emphasized the expected increase in differential gain compared with conventional bulk or quantum well (QW) materials, leading to expectations of very high-speed devices, as well as the possibility to accurately control the emission spectrum. However, the growth of QD-active material with control of the size of the QDs has turned out to be problematic. Self-organized crystal growth techniques have advanced, but the resulting materials are still characterized by a low confinement factor and relatively large degree of inhomogeneous broadening. This has been exploited to fabricate widely tunable devices [5], but renders the devices more bulk-like, e.g. leading to a relatively low differential gain. Also, the injection efficiency into the dots may be low, due to a reduced phase space for the capture processes.

Despite these problems, QD-active materials have resulted in lasers with record-low threshold current densities [6] and SOAs with record-high output powers [3, 7]. The main reason for these improvements is that only few states exist in each of the QDs (at least for the electrons) and population inversion is reached for a relatively low degree of pumping. Also, the internal loss can be very small for active waveguides based on QD material [8, 9]. As for SOAs, the wetting layer (WL), upon which the dots are formed due to strain, turns out to have a very important role, since it acts as a carrier reservoir that tends to reduce the effects of saturation otherwise seen in bulk or QW devices.

In this paper, we theoretically analyse the dynamics of QD SOAs, emphasizing the interplay between the active dot states and the WL. We base our analysis on a relatively simple model, with the advantage that simple, in some cases analytical, results may be obtained. The model is appropriate for understanding the consequences of having a large population of carriers in

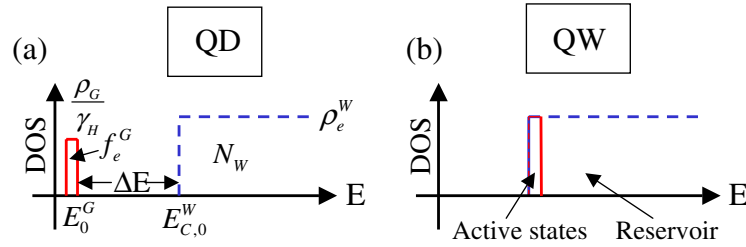


**Figure 1.** Schematic representation of the 2LREM: (a) symbols used in the model and (b) use of the model when applied to a QW operated at the bandedge.

the WL, which couples to discrete QD populations on a picosecond time-scale, while at the same time the two carrier populations undergo recombination processes, stimulated emission and pumping. It turns out that many of the effects seen can be qualitatively understood as the dynamics of a bulk system with a large, and to some extent controllable, degree of spectral hole burning (SHB).

We first introduce the model (section 2) and discuss the static properties of the system (section 3). A general small-signal analysis of the system is then undertaken (section 4) and applied to analyse the optical modulation response (section 5) as well as the four-wave mixing (FWM) properties (section 6).

## 2. The model

A simple model of a QD amplifier, which still retains most of the unique properties of QDs, is the two-level rate equation model (2LREM). The model, which includes one QD carrier population and one WL population, is illustrated schematically in figure 1(a). The density of states (DOS) for the QD states,  $\rho_G$ , is approximated by a delta function representing the optically active QD states and  $\rho_G$  is thus expressed in units of states per unit volume. The WL is approximated as a narrow QW with only a single conduction band bound state. Consequently, the WL DOS is represented by a step function of height  $\rho_W$  (in units of states per unit energy per unit volume). Both  $\rho_G$  and  $\rho_W$  are normalized with respect to the volume of the active region  $V$ . The delta function DOS,  $\rho_G$ , accounts for the optically active fraction of the QD ground states (GSs). Thus, for an inhomogeneously broadened ensemble, only QDs with a ground state transition energy within the homogeneous linewidth,  $\gamma_H$ , of the injected signal at  $E_0^G$  will interact directly with the signal. The homogeneous linewidth in QD devices at room temperature is of the order of 5 meV [10].  $\rho_G$  is approximated as

$$\rho_G = n_l D_{3D} \varepsilon_G \frac{\gamma_H}{\eta_G^{FWHM}}, \quad (1)$$

where  $\eta_G^{FWHM}$  is the FWHM of the inhomogeneous broadening of the GS transition,  $n_l$  the number of QD layers in the device,  $D_{3D}$  the 3D dot density of a single dot layer with respect to the volume  $V$  and  $\varepsilon_G$  the degeneracy of the GS of a single dot, which is 2 due to spin. In this approximation, the majority of the inhomogeneous broadening of the GS transition is assumed to arise from inhomogeneous broadening of the electron states. The presence of any QD state other than the GS is ignored and no intradot relaxation is therefore included in the model. The QD states are separated from the WL band edge by the energy  $\Delta E_G^W = E_{C,0}^W - E_0^G$ .

Due to the larger hole mass and resulting smaller state spacing we assume that the dynamical properties are limited by electron dynamics and that the hole dynamics can be neglected. We therefore account explicitly only for the electrons in the model. However, a large hole mass means that the inversion of the system is very different from the ideal device where both electron and hole masses are small. This effect is included by assuming overall charge neutrality of the system and assuming that the holes of the system are in quasi-thermal equilibrium with each other at all times. This approximation is discussed later in more detail.

The rate equations governing the time evolution of the electrons in this system are

$$\frac{dN_W}{dt} = \frac{I}{qV} - \frac{N_W}{\tau_W} - f_0^W(1 - f_e^G)\frac{\rho_G}{\tau_C} + \frac{f_e^G(1 - f_0^W)\rho_G}{\tau_{esc}}, \quad (2)$$

$$\frac{df_e^G}{dt} = \frac{f_0^W(1 - f_e^G)}{\tau_C} - \frac{f_e^G(1 - f_0^W)}{\tau_{esc}} - \frac{f_e^G}{\tau_G} - \frac{\widehat{g}L}{V\rho_G}(f_e^G + f_h^G - 1)\frac{P_G}{\hbar\omega_0}, \quad (3)$$

where  $I$  is the injected current,  $N_W$  the carrier density of the WL, which is also normalized with respect to the volume  $V$ ,  $\tau_G$  and  $\tau_W$  are the spontaneous recombination times of the QD GS and WL respectively,  $f_e^G$  and  $f_h^G$  are the electron and hole filling fractions of the QD states respectively,  $\widehat{g}$  is the maximum modal gain,  $L$  the length of one section of the amplifier,  $P_G$  the optical power of the signal injected at the centre of the GS transition and  $f_e^G$  the electronic GS occupation probability. The remaining parameters are described in the following.

The electron occupation probability at the edge of the WL,  $f_0^W$ , is related to the WL carrier density by

$$f_0^W = 1 - \exp\left(-\frac{N_W}{k_B T \rho_e^W}\right), \quad (4)$$

which is found by assuming a Fermi distribution of the carriers in the WL, solving for the WL Fermi energy and evaluating the Fermi function at the WL band edge.

The capture time,  $\tau_C$ , and the escape time are related through detailed balance considerations. Thus, assuming thermal equilibrium, we derive the following relation:

$$\tau_{esc} = \tau_C \exp\left(\frac{\Delta E_G^W}{k_B T}\right). \quad (5)$$

Capture is in this model described by a simple time constant, but the rate could also be modelled by a polynomial taking phonon [11] and Auger-assisted [12] processes into account [13].

The QD hole-state filling fraction,  $f_h^G$ , may be evaluated by using a bulk DOS for the hole states. Clearly, this is only a good approximation for large, bulk-like QDs, but even for small dots the approximation results in a physical scaling of the number of hole states compared with electron states and thus also a correct behaviour regarding the filling of dot states with current. The DOS of the QD holes,  $\rho_h^D$ , is thus expressed as

$$\rho_h^D = \frac{1}{2\pi^2} \left(\frac{2m_h}{\hbar^2}\right)^{3/2} \sqrt{E - E_V^D}, \quad (6)$$

where  $m_h$  is the hole mass and  $E_V^D$  the location of the lowest QD hole state. The WL DOS for the holes,  $\rho_h^{WL}$  is a traditional step function for a QW with a single bound state with the lowest state located at  $E_V^{WL}$ .

The Fermi energy of the valence band,  $E_{F,V}$ , which is needed to evaluate  $f_h^G$ , is found by assuming charge neutrality for the device as a whole. The following equation is thus solved for  $E_{F,V}$ :

$$f_e^G \rho_G + N_W = \int_{E_V^D}^{\infty} \left[ V_0^D \rho_h^D(E) \frac{\rho_G}{\varepsilon_G} + \frac{V_W}{V} \rho_h^{WL}(E) \right] \frac{1}{1 + \exp((E - E_{F,V})/k_B T)} dE, \quad (7)$$

where  $V_0^D$  is the volume of a single dot and  $V_W$  is the volume of the WL.

To evaluate the hole occupation probability for a given carrier density we specify the valence band energy,  $E_V^G$  involved in the GS transition. The hole occupation probability is then found as

$$f_h^G = \frac{1}{1 + \exp((E_V^G - E_{F,V})/k_B T)}. \quad (8)$$

The above equations describe the carrier dynamics at any specific point along the amplifier length. To describe correctly the overall device parameters (e.g. device gain or the saturation by amplified spontaneous emission), a propagation equation for the light intensity is needed. However, for the present purpose, such an equation is not required and therefore not given at this point. For the purpose of four-wave mixing (FWM) discussed in the last section of the paper, a propagation equation for the optical field is given.

The model may also be used to model a QW device simply by using different parameter values. This is illustrated in figure 1(b), where the optically active states (those previously denoted as the QD states) are located at the band edge of the QW (the previous WL), corresponding to a QW device operated at the band edge. In this case, the energy splitting,  $\Delta E_V^W$ , is set to zero and the number of active states per volume,  $\rho_G$ , is equal to the WL DOS multiplied by the homogeneous linewidth,  $\gamma_H$ , i.e.  $\rho_G = 2\rho_e^W \gamma_H$ . When modelling a QW device, the conditions  $E_V^D = E_V^{WL}$  and  $V_0^D = 0$  are used, when evaluating the valence band occupation probability  $f_h^G$ . The resulting model of a QW is similar to the local density model used for bulk and QW devices to model SHB [14].

For a description of more elaborate QD models see [7, 15].

### 3. Continuous wave (CW) properties of QD amplifiers

The above set of equations can be solved for the steady state assuming a CW signal, and the solution is

$$P_G = \frac{\rho_G V}{g_0} \left( \frac{f_0^W}{\tau_C} - f_e^G \left( \frac{1}{\tau_G} + \gamma_G \right) \right) \hbar \omega_0, \quad (9)$$

where

$$f_e^G = \frac{1}{\gamma_G \rho_G} \left( \frac{N_W}{\tau_W} - \frac{I}{qV} + f_0^W \frac{\rho_G}{\tau_C} \right), \quad (10)$$

$$g_0 = \hat{g} L (f_e^G + f_h^G - 1), \quad (11)$$

$$\gamma_G = \frac{f_0^W}{\tau_C} + \frac{1 - f_0^W}{\tau_{esc}}. \quad (12)$$

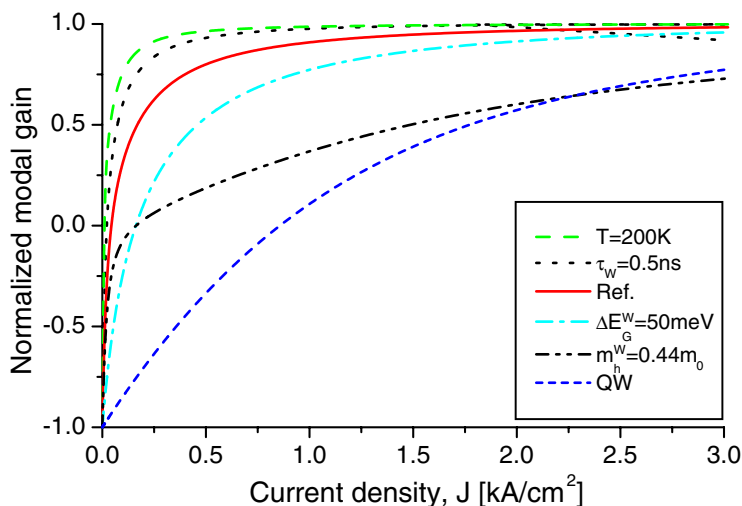


**Figure 2.** Normalized modal gain versus current density, calculated with the 2LREM for five different QD devices and a single QW for comparison. The parameter values used for the QD devices are listed in table A.1, with the exception of the parameters noted in the legend, and in table A.2 for the QW case.

From these equations we can gain insight into both the filling of the active states with current and the saturation power locally in a QD device. Many of the unique properties of QD amplifiers can be understood from these basic properties.

### 3.1. Filling of the active states

Figure 2 shows the normalized modal gain, corresponding to the inversion factor,  $f_e^G + f_h^G - 1$ , as function of current density for different QD devices and a single QW device. In all QD cases the same general parameter values are used (listed in table A.1), except for one parameter which is varied. For the QW device the parameter values given in table A.2 are used.

For the reference QD case (solid red line) the inversion is seen to increase nearly linearly with a large slope for small current densities, but then gradually starts to saturate as the active states become filled. The same fundamental behaviour is observed for the QW case (short dashed blue line), except that a much higher current is needed to reach the same level of inversion. The main reason for this difference is the higher density of active states in the QW case due to the higher DOS of a QW compared with the QD (when normalized with respect to the same volume). Another important difference is that the confinement energy of the QD states with respect to the WL ensures a small overlap between the carrier distribution function and the WL states at low currents, where the quasi-Fermi energy is far below the WL band edge for both electrons and holes. In contrast, for a QW device (or a bulk device), there is always a large number of states close to the active states and filling is therefore essentially controlled by these neighbouring states.

The coupling between the bound QD states and the carrier reservoir in the form of the WL states is essentially determined by the confinement energy relative to the thermal energy. This is illustrated by the green dashed line in figure 2, where the temperature is lowered from 300

to 200 K and by the dot-dashed cyan line where the conduction band confinement energy has been reduced from 100 to 50 meV. Clearly, a smaller separation between the active states and the reservoir relative to thermal energy leads to a stronger coupling of the two carrier populations and the filling of the QD states becomes more ‘QW-like’. To obtain a linear filling of the active states at room temperature it is therefore necessary to have deeply confined QD states.

For a device with a strong coupling to WL states, it is clear that the properties of the WL have a strong influence on the QD properties. This is illustrated by the black dotted line in figure 2, which shows the result of increasing the spontaneous recombination time of the WL from 0.2 to 0.5 ns. This effectively lowers the rate of carrier loss through the WL, which results in a more effective filling of the QD states. A high rate of recombination in the WL may be caused by defects, Auger recombination, or by amplified spontaneous emission (ASE). Especially, recombination due to defects in the WL has been shown to limit the performance of QD devices [16]–[19].

Also the effective carrier masses of the WL are important for the inversion of the QD states. Increasing the effective hole mass of the WL to  $0.44m_0$  results in a dramatic reduction of the QD inversion rate as illustrated by the black dot-dot-dashed line in figure 2. The large hole mass means that a much larger fraction of the carriers have to remain in the WL even at low current densities, which effectively increases the current needed to invert the QD states. This effect has been demonstrated experimentally by Matthews *et al* [20], who showed severe limitations of the obtainable modal gain of QD SOAs at room temperature and ascribed it to the reduction of the inversion with current due to a high effective hole mass in the WL.

The measured inversion of QD SOAs as function of current at room temperature reported in the literature, varies substantially and ranges from the slow filling reported by Matthews *et al* [20] to almost linear filling and sharp saturation reported by Borri *et al* [21]. Rapid and linear filling of the active states and corresponding sharp saturation is one of the unique properties of QD SOAs compared with higher dimensional devices.

The slopes of the curves in figure 2 are proportional to the differential gain in each case. It is thus clear that for the same QD device two distinctly different regimes exist. At low inversion (LI), the differential gain is high and more or less constant over a large current interval. For full inversion, however, the differential gain is very small and approaches zero for increasing current. Clearly this means that the two regimes are suited for different purposes. The low inversion (LI) regime allows for a large nonlinearity whereas the high inversion (HI) regime allows for minimal saturation effects and linear amplification.

### 3.2. Saturation power

The saturation power is the central parameter of an amplifier, which influences both the linear and non-linear properties strongly. It is defined as the optical power which reduces the modal gain to half of the unsaturated gain, i.e.  $g_{sat}(P_G = P_{sat}) = g_0(P_G = 0)/2$ .

For bulk and QW devices, the saturation power can be calculated in the case where the gain is assumed to scale linearly with carrier density (see e.g. [22]) with the result (notation modified):

$$P_{sat} = \hbar\omega_0 \frac{A}{g' \tau_{eff}}, \quad (13)$$

where  $A$  is the effective gain cross section,  $g' = dg/dN$  is the differential modal gain, and  $\tau_{eff}$  the effective carrier lifetime. Typical values for the saturation power in bulk and QW amplifiers are

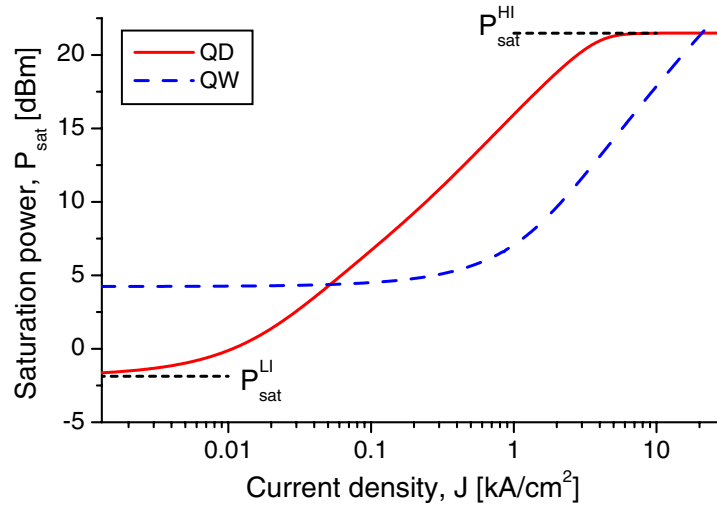


**Figure 3.** Calculated saturation power as a function of current density for a QD SOA and a QW SOA. The limiting saturation power at HI and LI, calculated with (15) and (17) are indicated with black dotted lines. Parameter values used are listed in tables A.1 (QD) and A.2 (QW).

0–10 dBm. This expression can be used to analyse the behaviour of the saturation power in the QD case and understand the essential differences between devices of different dimensionality.

In the case of QD amplifiers, the saturation power can be found from (9), which is valid for the unsaturated ( $P_G = 0$ ) as well as the saturated case with a finite optical power. In general, the equations cannot be solved analytically but approximations for the saturation power can be found in two limiting cases.

Figure 3 shows the saturation power as a function of current density for a QD and a QW device. For the QD device, the saturation power is nearly constant at small current densities, which we denote as the LI limit. For higher current densities, the saturation power increases approximately linearly with current. At current densities above a few  $\text{kA cm}^{-2}$ , the saturation power saturates in the HI limit. In comparison, the saturation power of the QW SOA (blue dashed line) is larger than for the QD device in the LI limit, which persists up to more than  $100 \text{ A cm}^{-2}$ . For current densities higher than those shown in the figure, the saturation power of the QW device does eventually also saturate in the HI limit corresponding to SHB, but due to the short time-constant for carrier–carrier scattering used ( $\tau_C = 0.1 \text{ ps}$ ), a very high optical power can be sustained before SHB sets in.

It should be pointed out that the model ignores all types of carrier loss such as leakage current and the current density required to reach these high saturation powers is thus underestimated. Especially, effects like Auger recombination and other types of carrier loss will limit the achievable inversion and thus also the maximum saturation power. Nonetheless, if we assume that the same level of inversion can be achieved in the two types of devices (e.g. corresponding to the  $1 \text{ kA cm}^{-2}$  point on the curve), it is clear that QD device will exhibit a larger saturation power than the QW device.

The point where the saturation power starts to increase with current corresponds roughly to the transparency point for the QD device, since the WL carrier density is increased significantly

as the quasi-Fermi level of the device approaches the WL band edge. The WL states thus act as carrier reservoir for the QD states and the filling of this reservoir ensures that a higher rate of stimulated emission can be supported before the gain is saturated. An increased inversion of the WL also corresponds to a decrease of the differential gain of the QD state as seen in figure 2. Since the saturation power scales linearly with the differential gain in all cases, the increase of the saturation can be viewed simply as a result of the decreasing differential gain.

To determine the parameters governing the saturation power in the LI and HI limits, we will derive approximate expressions for the saturation power in these limits. Using (9) the saturation power in the LI can be expressed as

$$P_{sat}^{LI} = \frac{\rho_G V \hbar \omega_0}{\widehat{g}L} \frac{(N_W^{sat} / \tau_W \rho_G) + (f_{e,sat}^G / \tau_G)}{1 - f_{e,sat}^G - f_{h,sat}^G}, \quad (14)$$

where  $f_{e,sat}^G$ ,  $f_{h,sat}^G$  and  $N_W^{sat}$  are the saturated values of the QD electron and hole occupation probability and the corresponding WL carrier density. Since, in this limit, the unsaturated inversion factor is equal to  $-1$ , the saturated inversion factor in the denominator of (14) must be equal to  $-0.5$ . The LI saturation power,  $P_{sat}^{LI}$ , can thus be found as

$$P_{sat}^{LI} = \frac{2\rho_G V \hbar \omega_0}{\widehat{g}L} \left( \frac{N_W^{sat}}{\tau_W \rho_G} + \frac{f_{e,sat}^G}{\tau_G} \right). \quad (15)$$

The term in parentheses corresponds to the total carrier recombination rate per QD:

$$R_{rec} = \frac{N_W^{sat}}{\tau_W \rho_G} + \frac{f_{e,sat}^G}{\tau_G} \approx \frac{f_{sat}}{\tau_{eff}}. \quad (16)$$

The value of the equivalent saturated carrier density per dot,  $f_{sat}$ , depends on the distribution of the generated electrons among the QD and WL states. Thus, for a device with large confinement energy, most of the carriers will remain in the QD and  $f_{sat} \approx f_{e,sat}^G$  and  $\tau_{eff} \approx \tau_G$ . For a device with a small confinement energy, however, most electrons will enter the WL before quasi-equilibrium is reached and therefore  $f_{sat} \approx N_W^{sat} / \rho_G$  and  $\tau_{eff} \approx \tau_W$ . In any case,  $f_{sat}$  in this limit is simply a number accounting for the effect of the redistribution of carriers and  $\tau_{eff}$  is a weighted effective carrier lifetime.

With this knowledge it may be seen that the expression in (15) actually matches the bulk expression apart from a factor of  $2f_{sat}$  when the differential gain is identified as  $g' = \widehat{g} / \rho_g$  and the cross section as  $A = V/L$ . The extra factor  $2f_{sat}$  actually corresponds to a modification of the differential gain. Thus a large value of  $f_{sat}$ , corresponding to weakly confined dots, leads to a decrease in the differential gain and strong confinement increases the differential gain.

In the HI limit, both the QD states and the WL band edge are completely filled. In this limit, a high optical power is needed to saturate the gain and under the influence of the resulting high rate of stimulated emission, the quasi-equilibrium between carriers in the WL and in the QD, present under weak inversion, breaks down. For a sufficiently high current density we can therefore assume  $\overline{f}_{e,sat}^G = 0.5$ ,  $\overline{f}_{0,sat}^W = 1$  and  $\overline{f}_{h,sat}^G = 1$ , since only electrons are allowed to deviate from quasi-equilibrium between the QDs and the WL. Inserting these values into (9), the saturation power under high inversion is found as

$$P_{sat}^{HI} = \frac{\rho_G V \hbar \omega_0}{\widehat{g}L} \frac{1}{2} \left( \frac{1}{\tau_C} - \frac{1}{\tau_G} \right). \quad (17)$$

The GS carrier lifetime may be neglected since it is normally much larger than the capture time and in this limit the gain saturation is solely determined by dot-WL hole burning. The amplification process is thus completely limited by the transport time into the active states and the saturation power cannot be increased any more by further increase of the bias current. It is interesting to note that the saturation power in the low and HI regimes are governed by similar expressions, where the only difference is that the GS carrier lifetime is replaced by the capture time from the barrier into the dots. Since the capture time is usually much smaller than the carrier lifetime, this means that the saturation power at high inversion will be much larger than at low inversion.

The record for saturated output power of an SOA is currently held by a QD SOA [3], which showed saturation powers of 19–24.5 dBm depending on the signal wavelength. These values agree reasonably with the values found in the HI limit (see figure 3). From the above discussion it is clear that the ability to increase the quasi-Fermi levels far above the active QD states and thus use the WL and barrier as carrier reservoirs in the amplification process, gives QD devices considerable advantages over bulk and QW devices. However, a lack of pattern effects for powers above the saturation power is also important for exploiting the high output power when amplifying data signals. Where bulk and QW SOA show large pattern effects when operated beyond this point, the QD SOA realized by Akiyama *et al* show minimal pattern dependence as the saturation point is approached. This effect has been theoretically addressed in detail in [23].

#### 4. Small signal analysis

To gain insight into the dynamical properties of QD amplifiers we perform a small signal analysis of the rate equations (2)–(3).

A harmonically modulated optical signal, with modulation frequency  $\Omega$ , is assumed to be injected into the amplifier at the wavelength corresponding to the GS transition. In the small-signal regime, the GS and WL carrier populations follow the modulation:

$$P_G = \bar{P}_G + \frac{1}{2}(\Delta P_G e^{i\Omega t} + \Delta P_G^* e^{-i\Omega t}), \quad (18)$$

where  $\Delta P_G$  is the complex amplitude of the modulation and  $\bar{P}_G$  is the average value. Furthermore, the WL band edge and GS hole occupation probabilities,  $f_0^W$  and  $f_h^G$ , are linearized as  $f_0^W = \bar{f}_0^W + f'_W(\Delta N_W e^{i\Omega t} + \Delta N_W^* e^{-i\Omega t})/2$  and  $f_h^G = \bar{f}_h^G + f'_{h,G}(\Delta f_e^G e^{i\Omega t} + \Delta f_e^{G*} e^{-i\Omega t})/2$ , where

$$f'_W = \left. \frac{df_0^W}{dN_W} \right|_{\bar{f}_0^W} \quad \text{and} \quad f'_{h,G} = \left. \frac{df_h^G}{df_e^G} \right|_{\bar{f}_h^G}. \quad (19)$$

The analytical expression for these derivatives are lengthy and therefore not written explicitly here. Inserting these linearizations in the rate equations (2)–(3) and solving for the steady state solution yields a separate set of equations for the CW and harmonic components.

The CW part of the solution is identical to (9), and the relations between the complex modulation amplitudes of the signal and the carrier populations are found as

$$\widetilde{\Delta N_W} = \widetilde{\Delta f_e^G} \frac{\rho_G \gamma_G}{j\Omega + \gamma_W}, \quad (20)$$

$$\widetilde{\Delta f_e^G} = \frac{\widetilde{\Delta P_G}}{\hbar \omega_0 \rho_G V} \frac{g_0(j\Omega + \gamma_W)}{\Omega^2 - j\Omega \gamma_1 - \gamma_2}, \quad (21)$$

with

$$\gamma_1 = \gamma_W + \gamma_G + \gamma_{st} \quad (22)$$

$$\gamma_2 = \gamma_W \gamma_{st} + \frac{\gamma_G}{\tau_W} \quad (23)$$

and

$$\gamma_{st} = \frac{1}{\tau_G} + \frac{\widehat{g}L}{V\rho_G} \frac{\overline{P}_G}{\hbar\omega_0} (1 + f'_{h,G}), \quad (24)$$

$$\gamma_W = \rho_G V \left[ \frac{f'_W(1 - \overline{f}_e^G)}{\tau_C} + \frac{\overline{f}_e^G f'_W}{\tau_{esc}} \right] + \frac{1}{\tau_W} \quad (25)$$

and  $\gamma_G$  is defined in (12).

These equations can be used to evaluate the dynamic properties of a QD amplifier when interacting with a modulated optical signal. Assuming that the gain of the device oscillates at the frequency of the incoming optical signal we can write the amplitude of the induced gain modulation as  $\widetilde{\Delta g} = \widehat{g}(1 + f'_{h,G})\widetilde{\Delta f}_e^G$ . From this we can define the optical modulation response, i.e. the amplitude and phase of the gain modulation relative to the amplitude and phase of the optical signal as

$$\frac{\widetilde{\Delta g}}{\widetilde{\Delta P}_G} = \widehat{g}(1 + f'_{h,G}) \frac{\widetilde{\Delta f}_e^G}{\widetilde{\Delta P}_G} = \frac{\widehat{g}(1 + f'_{h,G})}{\hbar\omega_0\rho_G V} \frac{g_0(j\Omega + \gamma_W)}{\Omega^2 - j\Omega\gamma_1 - \gamma_2}. \quad (26)$$

Before investigating the properties of the optical modulation response further, we will decompose the above expression in order to simplify the analysis:

$$\frac{\widetilde{\Delta g}}{\widetilde{\Delta P}_G} = \frac{1 + f'_{h,G}}{\hbar\omega_0\rho_G V} \frac{\widehat{g}g_0}{R_{CDP} - R_{SHB}} \left( \frac{\gamma_W + jR_{CDP}}{\Omega - R_{CDP}} - \frac{\gamma_W + jR_{SHB}}{\Omega - R_{SHB}} \right), \quad (27)$$

with the roots given as

$$R_{CDP} = \frac{j}{2}(\gamma_1 - \sqrt{\gamma_1^2 - 4\gamma_2}) \approx j\frac{\gamma_2}{\gamma_1}, \quad (28)$$

$$R_{SHB} = \frac{j}{2}(\gamma_1 + \sqrt{\gamma_1^2 - 4\gamma_2}) \approx j\gamma_1. \quad (29)$$

Here,  $\gamma_1^2 \gg \gamma_2$  has been assumed, which is a good approximation under normal operating conditions. Each of these roots are related to a physical mechanism. The first,  $R_{CDP}$ , describes the gain modulation arising from a change in the overall carrier density of the device, i.e. carrier density pulsation (CDP). The second root,  $R_{SHB}$ , describes the gain modulation arising when the quasi-equilibrium between the QD and WL carrier populations is broken, i.e. SHB or dot-barrier hole burning. The modulation response is thus a sum of an equilibrium component (CDP) and a non-equilibrium component (SHB), with separate characteristic times for the two components.

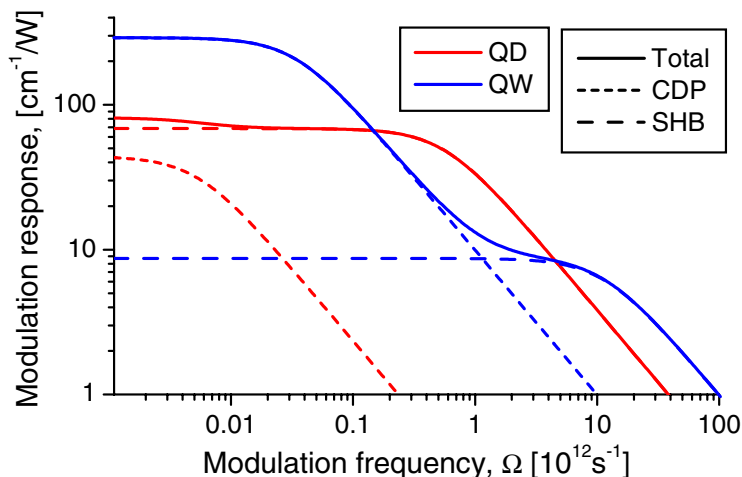


**Figure 4.** Absolute size of the optical modulation response versus modulation frequency for a QD and a QW SOA for a current of  $2 \text{ kA cm}^{-2}$  and an average optical power of 15 dBm. The short-dashed line depicts the CDP component, and the long-dashed line the SHB component. Parameter values are given in tables A.1 (QD) and A.2 (QW).

## 5. Optical modulation response

### 5.1. Size of the modulation response

The optical modulation response under different operating conditions can be used to gain insight into the signal processing properties of QD SOAs.

The absolute sizes of the optical modulation response of a QD and a QW SOA are depicted in figure 4 as a function of the modulation frequency of the optical signal,  $\Omega$ , when the average optical power is  $\bar{P}_G = 15 \text{ dBm}$ . For the QD device, which corresponds to the reference device in figures 2 and 3, the modulation response is seen to be nearly constant for frequencies up to  $10^{12} \text{ s}^{-1}$ . For both devices, the CDP and SHB components of the total response are shown. For the QD device, the CDP component is seen to be much weaker than the SHB component, reflecting the fact that for the applied current density of  $2 \text{ kA cm}^{-2}$ , the QD device is strongly inverted with a quasi-Fermi level above the WL band edge, resulting in only a weak QD GS gain modulation when the total carrier density of the device is changed. The characteristic frequency for the CDP component is in this case of the order of  $10^{10} \text{ s}^{-1}$ , corresponding to the inverse effective carrier lifetime with a significant contribution from the high rate of stimulated emission due to the high power level of  $\bar{P}_G = 15 \text{ dBm}$ . The limit to the SHB component is approximately  $5 \times 10^{11} \text{ s}^{-1}$ , which corresponds to the inverse of a capture time of 2 ps.

For the QW SOA, which is biased with the same current density, the CDP dominates completely for frequencies below  $10^{12} \text{ s}^{-1}$ . Due to the combination of a shorter effective carrier lifetime and a higher modal gain, resulting in a higher rate of stimulated emission, the characteristic frequency of the CDP component is almost an order of magnitude higher than that for the QD case. For the QW device at this current density, the quasi-Fermi level is only slightly above the WL band edge where the optical signal is injected, which results in a very efficient gain modulation, when the total carrier density is changed. This is the reason for the more efficient

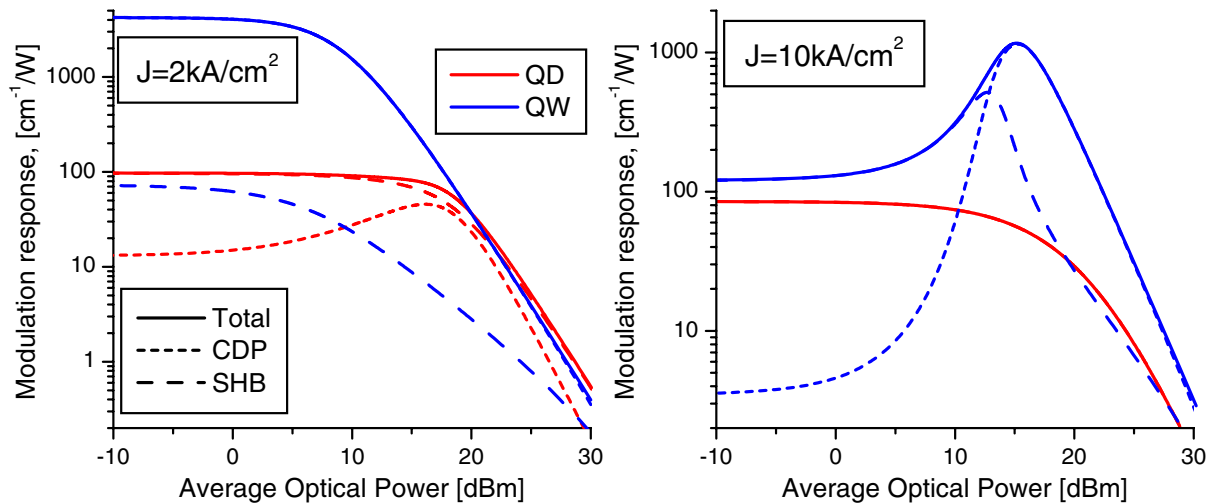


**Figure 5.** Absolute size of the low-frequency ( $\Omega \approx 0$ ) modulation response versus average optical power,  $\bar{P}_G$ , for the QD and the QW devices at a current density of  $2 \text{ kA cm}^{-2}$  (left) and  $10 \text{ kA cm}^{-2}$  (right). Parameter values in tables A.1 (QD) and A.2 (QW) have been used.

CDP gain modulation of the QW device compared with the QD device. At the same time, the SHB component is suppressed, since the short carrier-carrier scattering time of 0.1 ps used for the QW device allows for a rapid establishment of thermal equilibrium between the two carrier populations, effectively limiting the size of any spectral hole created by the optical signal.

The presence of a flat low-frequency plateau of the modulation response indicates the absence of pattern effects for signals with bit rates below the limiting frequency of the device. The presence of the strong CDP component for the QW device means that the CDP characteristic frequency becomes the limiting frequency for this device under these operating conditions. In contrast, the very limited CDP component for the QD device implies that the device can operate up to a significantly larger bit rate without introducing pattern dependence. Obviously, the sensitivity to fluctuating average power of the signal is also important, but as is shown in the following, it is possible to minimize the power sensitivity of QD SOAs by operating below the saturation power of the device.

Despite the simplicity of the rate equations, the resulting modulation response is surprisingly complex and the behaviour changes significantly under different operating conditions, which is illustrated by figure 5. The figure depicts the size of the low-frequency-modulation response, i.e.  $\Omega \ll R_{CDP}$ , as a function of the average optical power,  $\bar{P}_G$ , for the QD and QW considered previously for current densities of  $2 \text{ kA cm}^{-2}$  (left) and  $10 \text{ kA cm}^{-2}$  (right). Clearly, the change in current density results in a qualitatively different behaviour of the two devices.

For the low current density of  $2 \text{ kA cm}^{-2}$ , the response of the QD device is seen to be dominated by the SHB component. At low optical powers the response of the QD SOA is nearly independent of the optical power, reflecting the high inversion of the device, which suppresses the CDP gain modulation. Eventually, as the optical power approaches the saturation power of 19 dBm (see figure 3), the carrier density of the device is reduced and the quasi-Fermi level approaches the QD states, which allows for a more efficient CDP gain modulation. For optical powers beyond this point the device is forced towards transparency and, therefore, the amplitude

of the gain modulation decreases quickly. At these high optical powers, equilibrium between the QD and WL states cannot be retained and, as a consequence, the modulation is also in this regime dominated by the SHB component.

The QW device is oppositely dominated by the CDP component for all optical powers at the current density of  $2 \text{ kA cm}^{-2}$ . The device is not fully inverted at this current density and the CDP is, therefore, highly effective in modulating the gain. At the same time, the fast carrier–carrier scattering time of 0.1 ps results in a small amplitude of the SHB component for all optical power levels. Also in this case, optical power levels above the saturation power of 10 dBm, leads to a rapid decrease of the modulation efficiency.

The higher current density of  $10 \text{ kA cm}^{-2}$  does not change the picture much for the QD device, except by lowering the CDP component even further (it is not visible in the figure). For the QW SOA, however, the situation is very different. The saturation power is increased to 18 dBm and for optical power levels below this value the response is now dominated by the SHB due to the increased inversion, which suppresses the CDP component. Around the saturation power, however, the CDP component increases sharply and starts to dominate, which leads to a peak of the modulation response.

As evident from (26), the modulation response is proportional to the modal gain of the device and, as a result, the QW will have an advantage in this respect due to the higher modal gain. However, the difference can be compensated by increasing the device length. This should be taken into account when comparing the modulation efficiency for different devices.

The dependence of the modulation response on the average signal power is of importance for the pattern dependence of an amplifier. Thus, for both linear and nonlinear applications, it is important that the amplification or modulation properties do not change depending on the signal. The regimes of low optical power in figure 5, where the modulation response is constant are thus ideal in this respect. However, often a high signal power is desired. As a result, there is often a trade-off between pattern dependence and optical power. The high saturation power and SHB nature of the gain modulation of a QD SOA means that it can operate at high power levels without introducing pattern dependence, compared with the QW device. Furthermore, the SHB effect is operative to higher modulation frequencies than the CDP effect and, as a result, a QD SOA should be able to operate at higher speeds than a QW or bulk device where the gain modulation is mainly based on the CDP effect.

Pump–probe spectroscopy is an often used experimental technique to characterize the dynamic gain properties of active devices. Measurements on QD devices have shown different behaviour depending on the device and the operating conditions, varying from the observation of complete gain recovery in less than 1 ps [21] to a recovery including a significantly slow component determined by the effective carrier lifetime of the device [24, 25]. This difference can be understood from the above discussion of the optical modulation response. The fast component in the gain recovery thus corresponds to the SHB component in the response, whereas the slow component of the gain recovery corresponds to the CDP component. As seen in figure 5 the relative amplitude of the CDP and SHB components depends strongly on the bias current and average optical signal power. A fast and complete gain recovery therefore requires a device which is operated under high inversion, where the quasi-Fermi levels are far above the active QD states, corresponding to operating close to the bandedge in a bulk or QW amplifier. A fast and complete gain recovery in a QD SOA, therefore, does not in itself indicate a fast device capable of high-speed signal processing since the overall recovery of the device is still determined by the effective carrier lifetime [13], similar to the case of bulk and QW devices.

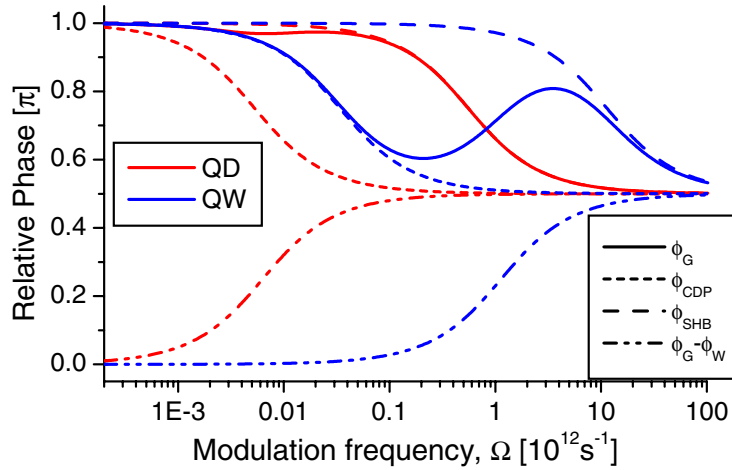


**Figure 6.** Phase of the total gain modulation and individual components relative to the optical signal phase for a current density of  $2 \text{ kA cm}^{-2}$  and optical power of  $15 \text{ dBm}$ . The dot-dot-dashed lines depict the phase difference between the modulation of the QD and WL carrier densities. Parameter values are listed in tables A.1 (QD) and A.2 (QW).

### 5.2. Phase of the modulation response

The angle,  $\phi_G$ , of the optical modulation response describes the phase of the gain modulation relative to the incoming optical field. Similar to the amplitude of the response, the phase behaviour is basically determined by the roots of the denominator of (26) given in (28) and (29). The phases of the two components (CDP and SHB) are thus given as

$$\tan \phi_{CDP} = -\frac{\Omega}{R_{CDP}} \quad \text{and} \quad \tan \phi_{SHB} = -\frac{\Omega}{R_{SHB}}. \quad (30)$$

Furthermore, there is a phase difference between the modulation of the carrier densities in the QD states and in the WL. The relative phase can be found from (20) as

$$\tan(\phi_G - \phi_W) = \frac{\Omega}{\gamma_W}, \quad (31)$$

where  $\phi_W$  is the phase of the WL carrier density modulation relative to the optical signal.

The relative phases corresponding to the examples shown in figure 4, are illustrated in figure 6. In all cases, the gain modulation has a phase of  $\pi$  relative to the signal at low-modulation frequencies, which reflects the fact that both devices at this current density are above transparency, i.e. an increase in photon number decreases the gain. For the QD device the CDP component has little influence on the total phase,  $\phi_G$ , due to the small amplitude of this component relative to SHB component. For the QW case, however, both components are important at different frequencies, which is seen to lead to a fluctuating phase. Eventually, for frequencies above the inverse capture time (carrier-carrier scattering time in the QW case), the gain is not able to keep up with the rapid modulation and is forced  $\pi/2$  out of phase.

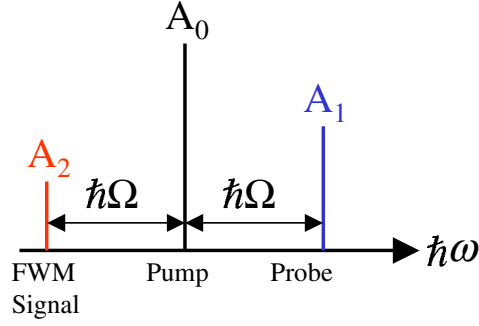


**Figure 7.** Schematic illustration of the relation between the pump, probe and FWM signal. The detuning frequency is here defined as  $\Omega = \Omega_1 - \Omega_0$ .

## 6. Four-wave mixing

### 6.1. A simple model

A CW pump and a CW probe signal are assumed to be injected into the QD SOA simultaneously, with complex field amplitudes  $A_0(z)$  and  $A_1(z)$ , and central optical frequencies  $\Omega_0$  and  $\Omega_1$ , respectively. The corresponding electric fields at the input facet are

$$E_0(z=0, t) = A_0(0)e^{i\Omega_0 t} \quad \text{and} \quad E_1(0, t) = A_1(0)e^{i\Omega_1 t}. \quad (32)$$

The beating of these two electric fields will generate a gain and index grating in the amplifier and a third signal, the FWM signal, with frequency  $\Omega_2 = 2\Omega_0 - \Omega_1$  and an amplitude  $A_2$  will be generated (figure 7). The sum of the three fields at any point along the amplifier can be written as

$$E(z, t) = A_0(z)e^{i\Omega_0 t} + A_1(z)e^{i\Omega_0 t} e^{i\Omega t} + A_2(z)e^{i\Omega_0 t} e^{-i\Omega t}, \quad (33)$$

where  $\Omega = \Omega_1 - \Omega_0$ . If the electric fields are normalized to have units of square root optical power, the total optical power can be found as

$$P_G(0, t) = |E(0, t)|^2, \quad (34)$$

$$\approx \bar{P}_G(z) + \frac{1}{2}(\widetilde{\Delta P}_G(z)e^{i\Omega t} + \widetilde{\Delta P}_G^*(z)e^{-i\Omega t}), \quad (35)$$

with  $\bar{P}_G(z) = |A_0(z)|^2 + |A_1(z)|^2 + |A_2(z)|^2$ , and  $\widetilde{\Delta P}_G(z) = 2A_0^*(z)A_1(z) + 2A_0(z)A_2^*(z)$ . All terms oscillating at frequency  $2\Omega$  have been neglected. The input power is seen to consist of a CW component,  $\bar{P}_G$ , and a harmonic component with amplitude  $\widetilde{\Delta P}_G$ , and frequency  $\Omega$ .

If the amplitude of the pump beam is much larger than any of the other two signals, the modulation of the optical signal becomes much smaller than the CW component, and the results of the small signal analysis in section 4 can be used. As a result, the response of the carrier density of the QD GS and the WL to the optical modulation can be used directly from (20) and (21) in the analysis.

In a retarded frame of reference, the propagation of the field envelope is governed by the equation [22]:

$$\frac{dA}{dz} = \frac{1}{2}(g - \alpha_{WG})A, \quad (36)$$

where  $\alpha_{WG}$  is the waveguide loss and we have assumed the linewidth enhancement factor to be negligible, i.e. no refractive index grating is included in this simple model. Low linewidth enhancement factors have been reported for QD devices [26, 27]. The simple description used here means that effects such as carrier heating, two-photon absorption, and the Kerr effect are not included in the model.

Inserting the expression for the GS gain and the slowly varying amplitude expressing the sum of the three optical fields:

$$g = \bar{g} + \frac{1}{2}[\widetilde{\Delta}g \exp(i\Omega t) + \widetilde{\Delta}g \exp(-i\Omega t)], \quad (37)$$

$$A = A_0 + A_1 \exp(i\Omega t) + A_2 \exp(-i\Omega t), \quad (38)$$

in the propagation equation and separating the terms depending on the oscillating frequency, three equations are obtained:

$$\frac{\partial A_0}{\partial z} = \chi_0 A_0 + \chi_1 A_2 + \chi_2 A_1, \quad (39)$$

$$\frac{\partial A_1}{\partial z} = \chi_1 A_0 + \chi_0 A_1, \quad (40)$$

$$\frac{\partial A_2}{\partial z} = \chi_2 A_0 + \chi_0 A_2, \quad (41)$$

with

$$\chi_0 = \frac{1}{2} \left( \frac{g_0}{L} - \alpha_{WG} \right), \quad (42)$$

$$\chi_1 = \frac{1}{4} \widetilde{\Delta}g, \quad (43)$$

$$\chi_2 = \frac{1}{4} \widetilde{\Delta}g^*, \quad (44)$$

where  $g_0$  is defined in (11) and  $\widetilde{\Delta}g$  in (26).

The propagation equations for the field are solved by discretization of the amplifier into a number of sections of length  $L_s$ , where all parameters are assumed constant over each section. The solution for a single step of the amplifier is found as

$$A_{0,s+1} = A_{0,s} e^{\chi_{0,s} L_s} + \frac{\chi_{1,s} A_{2,s} + \chi_{2,s} A_{1,s}}{\chi_{0,s}} [e^{\chi_{0,s} L_s} - 1], \quad (45)$$

$$A_{1,s+1} = A_{1,s} e^{\chi_{0,s} L_s} + \frac{\chi_{1,s} A_{0,s}}{\chi_{0,s}} [e^{\chi_{0,s} L_s} - 1], \quad (46)$$

$$A_{2,s+1} = A_{2,s} e^{\chi_{0,s} L_s} + \frac{\chi_{2,s} A_{0,s}}{\chi_{0,s}} [e^{\chi_{0,s} L_s} - 1], \quad (47)$$

where all subindices  $s$  indicate the connection to a specific amplifier section.

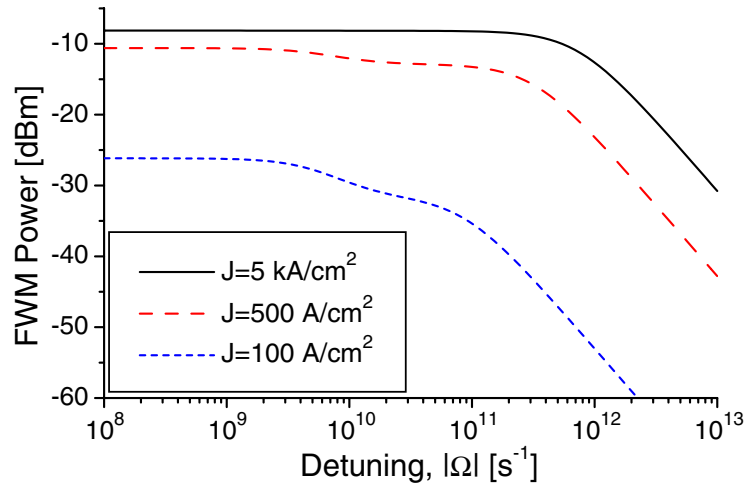


**Figure 8.** Calculated FWM output power versus detuning frequency for three different bias current densities. The device length is 4.6 mm and the remaining device parameters can be found in table A.1.

From this set of equations the evolution of the three signals in the direction of propagation can be found.

A similar, but more complete theoretical treatment of FWM properties can be found in [28].

## 6.2. FWM results

For a device with no coupling between gain and index changes, the interaction between the three signals is solely determined by the optical modulation response of the device. This can be seen in figure 8, which shows the FWM output power,  $P_2^{out}$ , as a function of detuning for three different current densities. The assumption of a negligible linewidth enhancement factor means that the FWM efficiency does not depend on the sign of the detuning. The pump and probe input powers are fixed at 0 and  $-10$  dBm, respectively. In all three cases the device length is 4.6 mm, which corresponds to a small signal gain of 20 dB under full inversion.

For the lowest current density of  $J = 100$  A cm $^{-2}$  (blue short-dashed line), the FWM output power is very low since the gain is low at this current. A relatively strong CDP component is visible at detunings smaller than  $5 \times 10^9$  s $^{-1}$ . This small value is caused by a long effective carrier lifetime resulting from the low rate of stimulated emission in this case. Also, the SHB component is limited to a lower detuning of approximately  $1 \times 10^{11}$  s $^{-1}$ , due to an effective capture time significantly above the minimum of 2 ps, since the WL band edge is not fully populated at this current density.

When the current density is increased, a larger FWM signal is generated due to the higher modal gain and at the same time the effective carrier lifetime and capture times decrease. The HI of the WL means that the CDP component is suppressed relative to the SHB component and for the highest current density of  $J = 5$  kA cm $^{-2}$  no CDP component is visible. It is clear that the current density has a large impact on both the qualitative and quantitative behaviour of FWM in these devices.

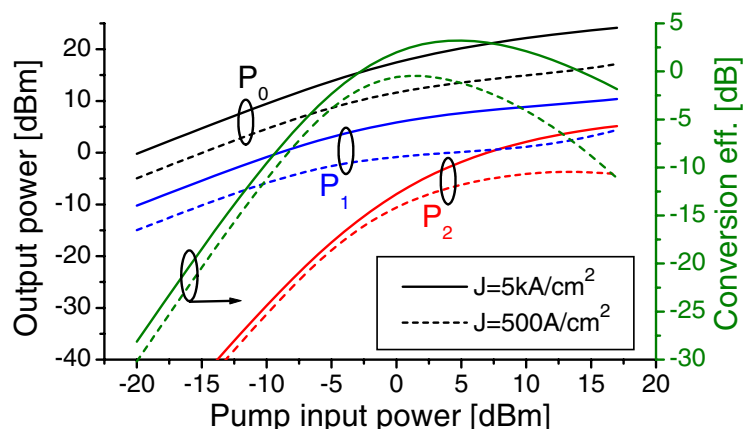


**Figure 9.** Output power of the pump ( $P_0$ ), probe ( $P_1$ ), and FWM ( $P_2$ ) signals and conversion efficiency as a function of the pump input power for a 4.6 mm long QD amplifier biased at two different current densities. The detuning is assumed low,  $\Omega \approx 0$ . The remaining device parameters can be found in table A.1.

Figure 9 shows the output power levels of the three signals  $P_0$  (pump),  $P_1$  (probe), and  $P_2$  (FWM signal) as a function of pump input power for two different current densities. The input power of the probe is in all cases fixed relative to the pump input power as  $P_1^{\text{in}} = P_0^{\text{in}}/10$ . The fact that the probe input power grows proportionally to the pump input power means that the generated FWM power increases monotonically with pump power, since the increased gain saturation at high pump powers is counteracted by the higher probe powers considered. No optimum pump power is thus found in this case. However, when looking at the conversion efficiency (green lines in figure 9), which is defined as  $P_2^{\text{out}}/P_1^{\text{in}}$ , it is clear that a maximum exists relative to the pump input power. For small pump input powers the conversion efficiency increases quadratically with pump power, but for high pump powers the gain saturation limits the conversion efficiency. The reduction of the modulation efficiency for optical power levels significantly larger than the saturation power is seen in figure 5.

From figure 9, the effect of increasing the current density from  $500 \text{ A cm}^{-2}$  to  $5 \text{ kA cm}^{-2}$  is seen to be an increase of the small signal gain from 15 to 20 dB. Another effect is that the saturation power is increased, which leads to significantly higher output powers of the pump and the probe signals. The increase by approximately 5 dB of these two signals could be expected to result in a 15 dB increase of the FWM signal in the regime with unsaturated gain, but this is clearly not the case. The explanation for this is that for the higher current density the gain modulation efficiency of the device is reduced somewhat at high optical power levels, as can be seen by comparing the high and low current examples in figure 5 for the QD device. This reduction counteracts the increase of the optical power of the pump and probe signals, resulting in only a modest increase of the FWM power. However, the increased saturation power means that for pump input powers higher than 0 dBm, a significant advantage is gained regarding conversion efficiency.

We will finally make a comparison to experimental FWM results on QD SOAs reported by Akiyama *et al* [29]. We thus modify the parameter values of the model to resemble more closely the device used in those experiments. We use the following values:  $n_l = 10$ ,  $\Delta E_C^W = 50 \text{ meV}$  and  $\tau_C = 1 \text{ ps}$ . The device length is assumed to be 25 mm, which results in a device gain of

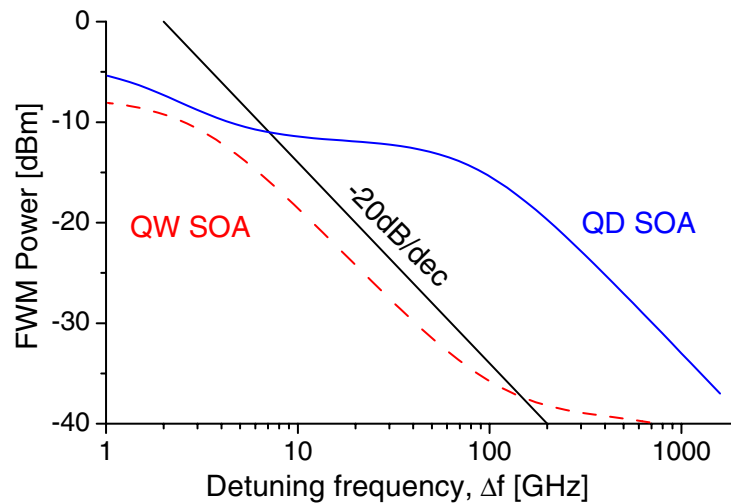


**Figure 10.** Comparison of FWM in a QD and a QW SOA regarding output power in the FWM signal as a function of detuning frequency. Device parameters are given in the text.

14 dB at the GS transition for a current density of  $1 \text{ kA cm}^{-2}$ . These values have been estimated from the available information on the experimental device and no fitting of parameters has been performed.

The resulting FWM output power, shown in figure 10 as a function of detuning frequency  $\Delta f = \Omega/2\pi$ , contains a CDP component, which is approximately 5 dB higher than the SHB component. The absolute value of the FWM signal is close to the experimental result in [29] and the qualitative behaviour is similar, except for the sharp drop at 1 THz in the experimental data. This drop-off is most likely caused by the effect of polarization dephasing an effect not included in the present model.

The red dashed line shows the calculated FWM output power for a QW SOA. The parameter values used in this case are listed in table A.2; as before, no index grating is included and the current density is  $2 \text{ kA cm}^{-2}$ . The FWM power is slightly smaller than that for the QD SOA at the peak and starts to decrease at a rate of  $20 \text{ dB dec}^{-1}$  above a detuning frequency of 2 GHz. At a detuning frequency of 200 GHz, the SHB component results in a plateau at  $-40 \text{ dBm}$ . The SHB component is much weaker in the QW case compared with the QD SOA due to the shorter capture time of 100 fs, determined by the carrier–carrier scattering. It is clear that for the operating conditions and device parameter values used here, the QD SOA shows significantly higher conversion efficiency, especially at the higher frequencies.

Comparing with the  $-20 \text{ dB dec}^{-1}$  line shown in figure 10 the QD FWM power can in some sense be viewed as decreasing by less than  $20 \text{ dB dec}^{-1}$ , since the SHB component creates a shoulder on the curve with higher conversion efficiency. An alternative interpretation is that the maximum detuning frequency is much larger and the  $-20 \text{ dB dec}^{-1}$  line should therefore be moved further out for a fair comparison. It should also be pointed out that even for bulk SOAs, a decay of less than  $20 \text{ dB dec}^{-1}$  is found experimentally [30] and the QD result is therefore not unique in this regard.

From the modelling results presented here, the enhanced SHB component in the gain modulation for a QD device is found to be a likely explanation for the good FWM performance

**Table A.1.** Model device parameters of a QD SOA.

Parameter	Value	Parameter	Value
$W$	$3 \mu\text{m}$	$m_e$	$0.026m_0$
$L$	$1 \text{ mm}$	$m_h$	$0.0742m_0$
$H$	$2004 \text{ nm}$	$T$	$300 \text{ K}$
$\tau_s$	$1 \text{ ns}$	$N_{2D}$	$4 \times 10^{10} \text{ cm}^{-2}$
$\tau_w$	$0.2 \text{ ns}$	$n_l$	$3$
$\tau_C$	$2 \text{ ps}$	$\gamma_H$	$5 \text{ meV}$
$\varepsilon_G$	$2$	$V_0^D$	$2.3 \times 10^{-24} \text{ m}^3$
$\widehat{g}$	$12 \text{ cm}^{-1}$	$\Delta E_G^W$	$100 \text{ meV}$
$\eta_G^{FWHM}$	$40 \text{ meV}$	$\alpha_{WG}$	$2 \text{ cm}^{-1}$
$E_V^D$	$0 \text{ meV}$	$E_V^G$	$42 \text{ meV}$
$E_V^{WL}$	$118 \text{ meV}$		

**Table A.2.** Model device parameters of a QW SOA.

Parameter	Value	Parameter	Value
$W$	$3 \mu\text{m}$	$m_e$	$0.026m_0$
$L$	$1 \text{ mm}$	$m_h$	$0.0742m_0$
$H$	$200 \text{ nm}$	$T$	$300 \text{ K}$
$\tau_G$	$0.2 \text{ ns}$	$n_l$	$3$
$\tau_w$	$0.2 \text{ ns}$	$\gamma_H$	$5 \text{ meV}$
$\tau_C$	$0.1 \text{ ps}$	$V_0^D$	$0 \text{ m}^3$
$\varepsilon_G$	$2$	$\Delta E_G^W$	$0 \text{ meV}$
$\widehat{g}$	$95 \text{ cm}^{-1}$	$\alpha_{WG}$	$10 \text{ cm}^{-1}$
$E_V^D$	$0 \text{ meV}$	$E_V^G$	$0 \text{ meV}$
$E_V^{WL}$	$0 \text{ meV}$		

found experimentally. In the simple model used here, only a single bound QD state is included, but the presence of several QD states and complex relaxation mechanisms could be expected to broaden the SHB shoulder due to the participation of multiple carrier relaxation processes instead of just a single one. This would bring the modelling results to resemble even closer the experimental results.

## 7. Conclusion

We have introduced a simple rate equation model to describe the interplay between discrete states of a quantum dot structure and a nearby reservoir of states in the form of a wetting layer. In spite of its simplicity, the model accounts for the main processes governing the dynamics of quantum dot semiconductor optical amplifiers. By analysing the steady state and the small-signal properties of the system, we show that the bandfilling properties of the combined dot-wetting layer system to a large degree govern the CW saturation properties of quantum dot semiconductor optical amplifiers. On the other hand, the fast dynamics of quantum dot devices depend critically

on the degree of non-equilibrium between the dot and wetting layer states and the time scale on which the two populations equilibrate. The main parameters affecting this interplay are identified, and the consequences for the optical modulation response and the FWM properties are investigated.

## Acknowledgments

This work was supported by the Danish Research Council and the European Commission through the IST projects BIGBAND and DOTCOM.

## Appendix. Parameter values

The parameter values are chosen to represent a ‘typical’ example of each device and they are presented in tables A.1 and A.2. The values chosen for the QD device are appropriate to the device presented in [21]. Device parameters not available from this reference have been estimated from similar devices in the literature. The values for the QW device are chosen to illustrate the main differences between QD and QW devices, i.e. a faster capture time (corresponding to a faster equilibration of a spectral hole), higher modal gain and faster carrier recombination.

## References

- [1] Bimberg D and Ledentsov N 2003 *J. Phys.: Condens. Matter* **15** R1063
- [2] Reithmaier J and Forchel A 2002 *IEEE J. Sel. Top. Quantum Electron.* **8** 1035
- [3] Akiyama T *et al* 2004 *Proc. OFC 2004* Post-deadline paper PDP12
- [4] Asada M, Miyamoto Y and Suematsu Y 1986 *IEEE J. Quantum Electron.* **QE-22** 1915
- [5] Varangis P *et al* 2000 *Electron. Lett.* **36** 1544
- [6] Liu G *et al* 2000 *IEEE J. Quantum Electron.* **36** 1272
- [7] Berg T and Mørk J 2003 *Appl. Phys. Lett.* **82** 3083
- [8] Klopff F *et al* 2001 *Electron. Lett.* **37** 353
- [9] Sellin R, Ribbat C, Grundmann M, Ledentsov N and Bimberg D 2001 *Appl. Phys. Lett.* **78** 1207
- [10] Borri P *et al* 1999-I *Phys. Rev. B* **60** 7784
- [11] Magnusdottir I, Uskov A, Bischoff S, Tromborg B and Mork J 2002 *J. Appl. Phys.* **92** 5982
- [12] Magnusdottir I, Bischoff S, Uskov A and Mork J 2003 *Phys. Rev. B* **67** 205326
- [13] Berg T, Bischoff S, Magnusdottir I and Mork J 2001 *IEEE J. Photon. Technol. Lett.* **13** 541
- [14] Mork J and Mecozzi A 1996 *J. Opt. Soc. Am. B* **13** 1803
- [15] Berg T 2004 *PhD Thesis* Technical University of Denmark
- [16] Zhang L *et al* 2000 *Appl. Phys. Lett.* **76** 1222
- [17] Riedl T, Fehrenbacher E, Hangleiter A, Zundel M and Eberl K 1998 *Appl. Phys. Lett.* **73** 3730
- [18] Sugawara M, Mukai K and Nakata Y 1999 *Proc. SPIE—Int. Soc. Opt. Eng.* **3628** 252
- [19] Park G, Huffaker D, Zou Z, Shchekin O and Deppe D 1999 *IEEE J. Photon. Technol. Lett.* **11** 301
- [20] Matthews D, Summers H, Smowton P and Hopkinson M 2002 *Appl. Phys. Lett.* **81** 4904
- [21] Borri P *et al* 2000 *IEEE J. Photon. Technol. Lett.* **12** 594
- [22] Agrawal P and Olsson N 1989 *IEEE J. Quantum Electron.* **25** 2297
- [23] Uskov A, Berg T and Mork J 2004 *IEEE J. Quantum Electron.* **40** 306
- [24] Bakonyi Z *et al* 2003 *IEEE J. Quantum Electron.* **39** 1409
- [25] Quochi F *et al* 2003 *Phys. Rev. B* **67** 235323

- [26] Newell T *et al* 1999 *IEEE J. Photon. Technol. Lett.* **11** 1527
- [27] Ghosh S, Pradhan S and Bhattacharya P 2002 *Appl. Phys. Lett.* **81** 3055
- [28] Qasaimeh O 2004 *IEEE J. Photon. Technol. Lett.* **16** 993
- [29] Akiyama T *et al* 2002 *IEEE J. Photon. Technol. Lett.* **14** 1139
- [30] Zhou J *et al* 1994 *IEEE J. Photon. Technol. Lett.* **6** 50